From the Society for Vascular Surgery

Patient-specific changes in aortic hemodynamics is associated with thrombotic risk after fenestrated endovascular aneurysm repair with large diameter endografts

Kenneth Tran, MD,[a,b] K. Brennan Feliciano, BS,[c] Weiguang Yang, PhD,[b,d] Erica L. Schwarz, MA,[c] Alison L. Marsden, PhD,[b,c,d] Ronald L. Dalman, MD,[a,b] *and* Jason T. Lee, MD,[a,b] *Stanford, CA*

ABSTRACT

Background: The durability of fenestrated endovascular aneurysm repair (fEVAR) has been threatened by thrombotic complications. In the present study, we used patient-specific computational fluid dynamic (CFD) simulation to investigate the effect of the endograft diameter on hemodynamics after fEVAR and explore the hypothesis that diameter-dependent alterations in aortic hemodynamics can predict for thrombotic events.

Methods: A single-institutional retrospective study was performed of patients who had undergone fEVAR for juxtarenal aortic aneurysms. The patients were stratified into large diameter (34-36 mm) and small diameter (24-26 mm) endograft groups. Patient-specific CFD simulations were performed using three-dimensional paravisceral aortic models created from computed tomographic images with allometrically scaled boundary conditions. Aortic time-averaged wall shear stress (TAWSS) and residence time (RT) were computed and correlated with future thrombotic complications (eg, renal stent occlusion, development of significant intraluminal graft thrombus).

Results: A total of 36 patients (14 with a small endograft and 22 with a large endograft) were included in the present study. The patients treated with large endografts had experienced a higher incidence of thrombotic complications compared with small endografts (45.5% vs 7.1%; $P = .016$). Large endografts were associated with a lower postoperative aortic TAWSS (1.45 ± 0.76 dynes/cm^2 vs 3.16 ± 1.24 dynes/cm^2; $P < .001$) and longer aortic RT (0.78 ± 0.30 second vs 0.34 ± 0.08 second; $P < .001$). In the large endograft group, a reduction >0.39 dynes/cm^2 in aortic TAWSS demonstrated discriminatory power for thrombotic complications (area under the receiver operating characteristic curve, 0.77). An increased aortic RT of ≥0.05 second had similar accuracy for predicting thrombotic complications (area under the receiver operating characteristic curve, 0.78). The odds of thrombotic complications were significantly higher if patients had met the hemodynamic threshold changes in aortic TAWSS (odds ratio, 7.0; 95% confidence interval, 1.1-45.9) and RT (odds ratio, 8.0; 95% confidence interval, 1.13-56.8).

Conclusions: Patient-specific CFD simulation of fEVAR in juxtarenal aortic aneurysms demonstrated significant endograft diameter-dependent differences in aortic hemodynamics. A postoperative reduction in TAWSS and an increased RT correlated with future thrombotic events after large-diameter endograft implantation. Patient-specific simulation of hemodynamics provides a novel method for thrombotic risk stratification after fEVAR. (JVS—Vascular Science 2022;3:219-29.)

Clinical Relevance: The durability of fenestrated endovascular aneurysm repair (fEVAR) has been threatened by thrombotic complications. Using patient-specific computational flow simulation, the present retrospective study of 36 patients with juxtarenal aortic aneurysms treated with fEVAR identified several endograft diameter-dependent changes in aortic hemodynamics associated with thrombotic complications. A postoperative reduction in aortic wall shear stress and increased particle residence time correlated with the development of intraluminal graft thrombus and renal stent occlusion in patients treated with large diameter (>34 mm) endografts. These computationally estimated hemodynamic parameters could provide a novel method for patient-specific risk stratification for adverse events after fEVAR.

Keywords: Aortic hemodynamics; Computational fluid dynamics; Fenestrated EVAR

From the Division of Vascular Surgery,[a] Cardiovascular Institute,[b] Department of Bioengineering,[c] and Department of Pediatrics (Cardiology),[d] Stanford University School of Medicine.

K.T. received support from the National Institutes of Health (grant 2T32HL09804911).

Author conflict of interest: none.

Presented at the Vascular Research Initiatives Conference at the 2021 Vascular Annual Meeting, Society for Vascular Surgery, August 19-20, 2021, San Diego, CA.

Correspondence: Kenneth Tran, MD, Department of Vascular Surgery, Stanford University School of Medicine, 300 Pasteur Dr, Ste H3600, Stanford, CA 94305-5851 (e-mail: kenneth.tran@stanford.edu).

The editors and reviewers of this article have no relevant financial relationships to disclose per the JVS-Vascular Science policy that requires reviewers to decline review of any manuscript for which they may have a conflict of interest.

2666-3503

https://doi.org/10.1016/j.jvssci.2022.04.002

Fenestrated endovascular aneurysm repair (fEVAR) has emerged as a minimally invasive alternative to open repair of abdominal aortic aneurysms with a hostile infrarenal neck.[1] Although initially reserved for patients at high physiologic risk, the use of fEVAR has increased to include more fit, lower risk patients owing to increased operator experience and studies demonstrating favorable short- and mid-term outcomes.[2,3] However, the long-term durability of fEVAR has remained a concern owing to the one-in-five risk of reintervention secondary to branch-related adverse events. These risks include renal branch graft thrombosis, which is associated with significant morbidity.[4,5] A previous observational study has shown that larger diameter fEVAR endografts result in a higher risk of branch thrombosis and reintervention compared with smaller diameter endografts.[6] The structural and hemodynamic factors underlying this thrombotic risk, however, are not well understood.

Computational fluid dynamic (CFD) modeling is a numerical analytic method that enables simulation and quantification of the interaction between a fluid and a structure. Initially used in the field of aerodynamic engineering, CFD simulation has recently found applications in cardiovascular disease modeling, with measurement of simulated hemodynamic parameters validated in both in vitro and in vivo models for a variety of cardiovascular pathologies.[7–9] At present, CFD modeling techniques have seldom been applied to study hemodynamics after fEVAR.[10,11]

In the present retrospective study, we used patient-specific CFD simulations to investigate the hemodynamic differences in patients undergoing fEVAR with small vs larger diameter endografts. We hypothesized that postoperative changes in local time-averaged wall shear stress (TAWSS) and particle residence time (RT) might explain the increased thrombotic risk associated with large-diameter fEVAR endograft implantation. Identifying patient-specific hemodynamic predictors of graft thrombosis would have the potential to improve both preoperative planning and postoperative risk stratification.

ARTICLE HIGHLIGHTS

- **Type of Research:** A retrospective computational flow simulation of single-institutional data
- **Key Findings:** Large diameter (34-36 mm) fenestrated endovascular aneurysm repair (fEVAR) was associated with a higher incidence of composite thrombotic complications compared with small endografts (45.5% vs 7.1%; $P = .016$). In the large endograft group, a >0.39 dynes/cm^2 postoperative reduction in paravisceral aortic time-averaged wall shear stress (TAWSS) and >0.05-second longer aortic residence time (RT) predicted for future thrombotic complications (area under the receiver operating characteristic curve, 0.77-0.78). The odds of thrombotic complications were significantly higher if the patient had met the threshold hemodynamic changes in aortic TAWSS (odds ratio, 7.0; 95% confidence interval, 1.1-45.9) and RT (odds ratio, 8.0; 95% confidence interval, 1.1-56.8).
- **Take Home Message:** Postoperative reduction in TAWSS and increased RT correlated with future thrombotic events after large-diameter fEVAR graft implantation. Patient-specific simulation of hemodynamics provided a novel method of thrombotic risk stratification after fEVAR.

METHODS

Patient cohort. A retrospective study was performed using a database of consecutive patients who had undergone elective fEVAR for juxtarenal aortic aneurysms at a single institution from 2012 to 2019. All the patients had received the Zenith fenestrated (ZFEN) endograft (Cook Medical Inc, Bloomington, IN) and bilateral renal bridging stents (Atrium iCAST; Atrium Medical Corp, Hudson, NH; or Viabahn VBX; W.L. Gore & Associates, Flagstaff, AZ). Only patients with an initial postoperative computed tomography angiography (CTA) scan performed within 30 days of the procedure and at least one subsequent follow-up CTA were included. To investigate the relationship between the endograft diameter and aortic hemodynamics, the cohort was stratified into two groups—a small endograft cohort consisting of patients with graft diameters ranging from 24 to 26 mm, and a large endograft cohort consisting of patients with a graft diameter ranging from 34 to 36 mm. For the present study, endograft diameters of 28 to 32 mm were excluded. All the patients meeting these criteria were included in the present analysis. To investigate the relationship between hemodynamics and thrombotic events, additional stratification by the presence or absence of postoperative thrombotic complications was performed within the large endograft group only to reduce endograft diameter-dependent bias. Our institutional review board approved the present study. Owing to the retrospective nature of the present study, the requirement for written informed consent was waived.

Clinical data. All the patients had undergone pre- and annual postoperative CTA with a high-resolution scanner with a slice thickness of 0.8 to 1.25 mm. The preoperative CTA images were used to construct three-dimensional (3D) models of native aneurysm morphology. The first postoperative CTA (<30 days postoperatively) was used to construct baseline stent graft models, which were uniformly absent of thrombotic findings. The presence of future thrombotic complications was assessed from subsequent follow-up CTA scans performed after ≥ 3 months postoperatively. Composite thrombotic complications were defined as the presence of either

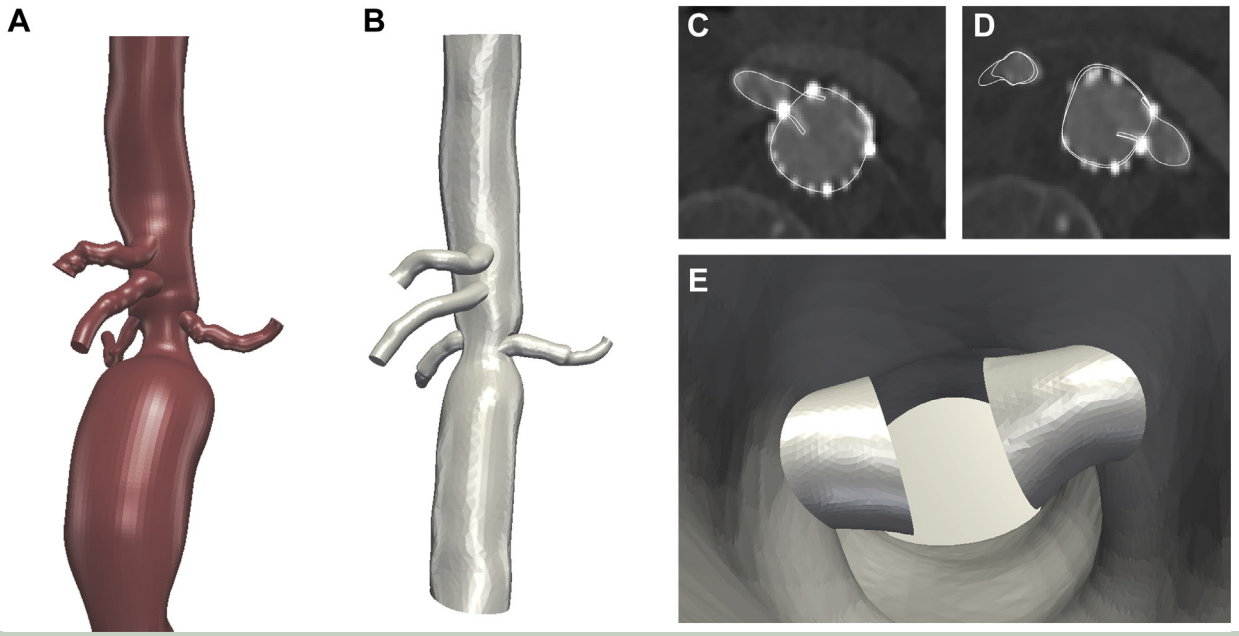

Fig 1. Three-dimensional aortic models extracted from computed tomography angiography (CTA) images: preoperative anatomy (**A**), postoperative anatomy (**B**), axial view of right renal flared branched geometry (**C**), axial view of left renal flared branch graft (**D**), and intraluminal rendering of pararenal aorta depicting changes in renal and aortic geometry at location of renal fenestrated branch grafts (**E**).

significant intraluminal aortic thrombus (>2-mm thickness and 25% circumferential coverage[12]), thrombotic occlusion of renal stents, or evidence of distal thromboembolism to the lower extremities. The average outpatient systolic and diastolic blood pressure, heart rate, height, and weight were collected to estimate the allometrically scaled inflow hemodynamics.[13]

Finite element mesh generation. Extraction of aortic geometry and finite element analysis for hemodynamics were completed using an open source package SimVascular (available at: https://simvascular.github.io/).[14,15] In brief, the aortic geometry was segmented from the midthoracic aorta until the aortic bifurcation, with the origins of the celiac, superior mesenteric (SMA), renal arteries segmented until the first major arterial branch. Two-dimensional segmentations were then lofted into 3D models and meshed into linear tetrahedral elements. Care was taken to accurately model the intraluminal protrusion of flared renal branch grafts (Fig 1). A 0.5-mm minimum mesh size was used for all areas of interest (eg, paravisceral aorta and branches) based on previous mesh convergence studies indicating a <1% variance in the derived pressure and flow values and a <5% variance in the locally measured TAWSS.[16] Areas outside the area of interest were meshed to 1.0 mm to decrease the computational requirements. The models used for analysis had 6 to 8 million tetrahedral mesh elements.

Computational flow simulation. Pre- and postoperative patient-specific flow simulations were performed with equivalent inflow and outflow conditions. A pulsatile inflow waveform was prescribed at the aortic inlet. The in-flow velocity was individually scaled to the patient body surface area and heart rate.[13] Three-element resistor capacitor resistor models (ie, Windkessel models) were used to represent vessels distal to the 3D model outlets and were individually tuned to match patient-specific arterial blood pressure.[17] High resistance (eg, mesenteric and distal aortic outlets) and low resistance (eg, renal outlets) vascular beds were modeled with 94.4% and 72% of total resistance assigned to the distal resistor, respectively.[18] Renovisceral arterial branch flow splits (25% for the celiac artery, 31% for the SMA, 22% for each renal artery) were based on physiologic values obtained from prior population samples.[17,19]

Blood flow simulations were performed by solving incompressible Navier-Stokes equations using a stabilized finite element solver.[20] Blood viscosity was assumed to be Newtonian, with a viscosity of 0.04 Poise and density of 1.06 g/cm^3. Walls were defined as rigid with a no-slip boundary condition. Simulations were run for a total of five cardiac cycles with a step size of 0.002 second (~1/500th of a cardiac cycle), with a <1% difference in the measured hemodynamic values between the fourth and fifth cycle. The results from the last cardiac cycle were then analyzed with a sampling frequency of 50 per cycle. The minimum residual value in the equation solver was set to 1×10^{-5}, which equates to well-converged numerical outputs. Simulations were performed on a high-performance 72-node cluster with

Table. Baseline demographic, anatomic, and outcome characteristics

Variable	Total cohort (n = 36)	Small endograft (n = 14)	Large endograft (n = 22)	*P* value[a]
Demographics				
Age, years	73.6 ± 1.1	73.5 ± 1.9	73.8 ± 1.3	.90
Male sex	31 (92.9)	13 (92.9)	18 (81.8)	.35
SVS comorbidity severity score	9.8 ± 5.1	9.8 ± 5.5	10 ± 4.9	.78
Active tobacco use	1 (2.7)	0 (0)	1 (4.5)	.42
Dual antiplatelet therapy	5 (13.9)	2 (14.3)	3 (13.6)	.95
Oral anticoagulation therapy	2 (5.6)	0 (0)	2 (9.1)	.24
Systolic blood pressure, mm Hg	134.8 ± 14.5	135.6 ± 10.7	134.3 ± 16.7	.78
Mean arterial pressure, mm Hg	95.8 ± 9.7	96.8 ± 6.3	95.3 ± 11.4	.68
Heart rate, beats/min	70.2 ± 11.7	70.3 ± 9.5	70.2 ± 13.1	.99
Height, cm	174.8 ± 7.51	175.3 ± 6.7	174.6 ± 8.1	.80
Weight, kg	83.8 ± 17.8	80.3 ± 18.3	86.1 ± 17.4	.36
Anatomic and device variables				
Aneurysm diameter, mm	59.0 ± 7.95	55.7 ± 4.9	61.1 ± 8.8	**.04**
Suprarenal neck diameter, mm	27.8 ±4.8	22.8 ± 2.8	30.9 ± 2.7	**<.001**
Neck angulation, °	24.6 ± 4.9	31.5 ± 22.9	20.3 ± 12.0	.07
Postoperative seal length, mm	33.1 ± 6.6	33.6 ± 4.7	32.9 ± 7.7	.76
SVS pelvic perfusion score				.44
0-I (absent to mild disease)	33 (91.7)	12 (85.7)	21 (96.4)	
II-III (moderate to severe disease)	3 (8.3)	2 (14.3)	1 (4.6)	
SVS iliac occlusive score				.33
0-I (absent to mild disease)	35 (97.2)	13 (92.9)	22 (100.0)	
II-III (moderate to severe disease)	1 (2.8)	1 (7.1)	0 (0)	
Outcomes				
Reintervention	11 (30.5)	2 (14.9)	9 (40.9)	.09
Type Ia endoleak	1 (2.8)	0 (0)	1 (4.5)	.61
Composite thrombotic complications	11 (30.5)	1 (7.1)	10 (45.5)	**.016**
Renal stent occlusion	5 (13.9)	1 (7.1)	4 (18.2)	.34
Aortic graft luminal thrombus	7 (19.4)	0 (0)	7 (31.8)	**.02**
Distal thromboembolic events	0 (0)	0 (0)	0 (0)	
All-cause mortality	4 (11.1)	1 (7.1)	3 (13.6)	.54

SVS, Society for Vascular Surgery.
Data presented as mean ± standard deviation or number (%).
Boldface *P* values represent statistical significance.
[a] *P* values reflect comparison between small and large diameter cohorts; calculated *P* values obtained using the Student *t* test for continuous variables and the Fisher exact test for categorical variables.

an approximate computational time of 36 to 48 hours per simulation.

Hemodynamic parameters, including pressure waveforms, flow rates, and TAWSS, were then calculated within the paravisceral aorta and its branches. The paravisceral aorta was defined as the aortic segment 1.0 cm above the celiac artery and 1.0 cm below the lowest renal artery. The particle residence time (RT), a spatially averaged measure of the amount of time a fluid parcel spends in a region of interest, was then calculated in the paravisceral aorta by solving an advection–diffusion transport equation in an Eulerian framework.[21] Individual patient changes in aortic TAWSS (ΔTAWSS) and RT (ΔRT) were defined as the difference in the values between the pre- and postoperative simulations. The Paraview Visualization ToolKit (available at: https://www.paraview.org/) was used for 3D visualization of the hemodynamic parameters.

Statistical analysis. The hemodynamic variables were compared between groups and analyzed using Wilcoxon rank sum tests for variables with a non-normal distribution and *t* tests for normally distributed variables. Receiver operating characteristic curves and the corresponding area under the curve (AUC) were used to determine the discriminatory power, with the optimal

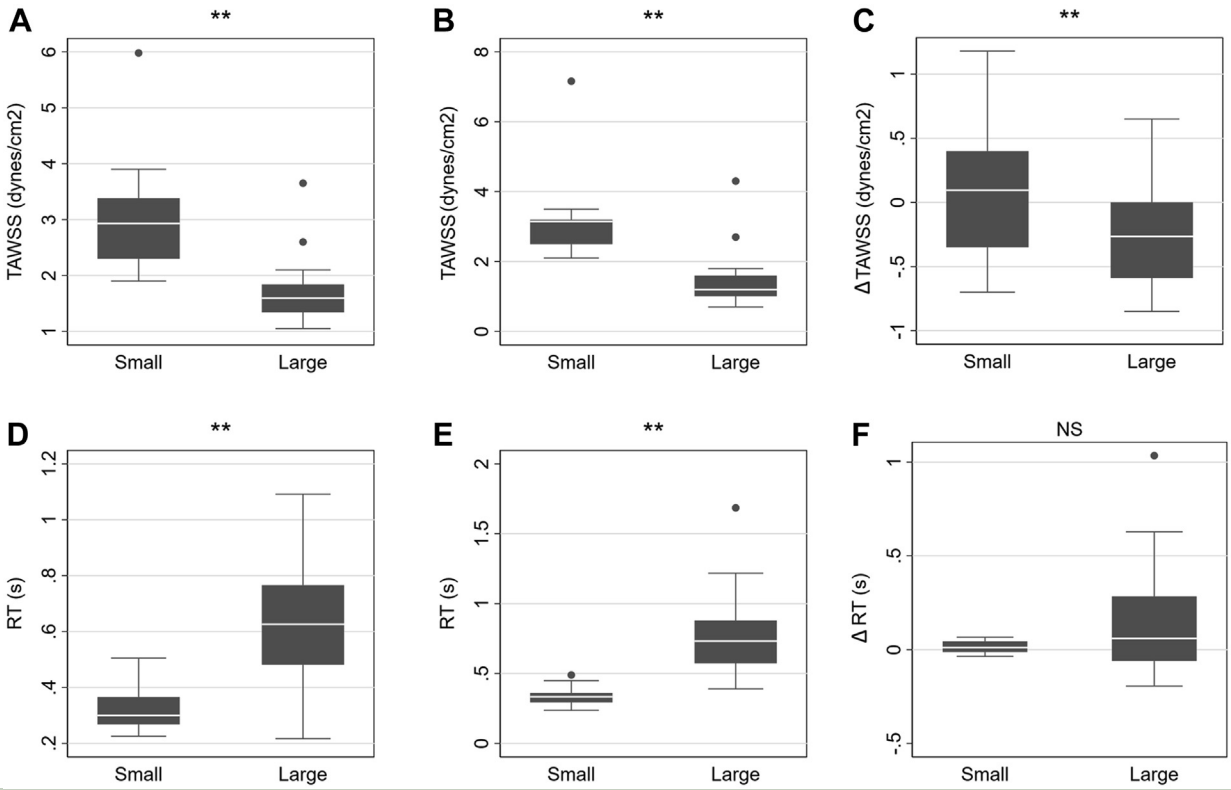

Fig 2. Analysis of aortic hemodynamic metrics between large and small diameter endografts. **A,** Preoperative aortic time-averaged wall shear stress (TAWSS). **B,** Postoperative TAWSS. **C,** Change in TAWSS (ΔTAWSS). **D,** Preoperative aortic residence time (RT). **E,** Postoperative aortic RT. **F,** Change in aortic RT (ΔRT). *Large,* Large endograft; *NS,* nonsignificant; *Small,* small endograft. *$P < .05$; **$P < .01$.

cutoff threshold value determined by the maximum of the Youden J statistic. Odds ratios (ORs) were calculated using logistic regression models. A P value <.05 was considered statistically significant for all analyses. All statistical analyses were performed in Stata, SE16.0 (StataCorp LP, College Station, TX).

RESULTS

Patient-specific 3D modeling and computational flow simulations were performed for 36 patients (14 with a small endograft and 22 with a large endograft) who had undergone fEVAR. The patient demographics, anatomic and device characteristics, and selected outcomes are shown in the Table. The mean follow-up was 30.1 months. No significant differences were found in Society for Vascular Surgery comorbidity score, antithrombotic therapy, blood pressure, heart rate, or body habitus between the two groups. The patients in the large endograft group had had larger aneurysms (maximum diameter, 61.1 ± 8.8 mm vs 55.7 ± 4.9 mm, respectively; $P = .04$) and larger suprarenal neck diameters (30.9 ± 2.7 mm vs 22.6 ± 2.8 mm; $P < .001$). Late renal stent occlusion occurred in five patients (13.9%) and significant mural thrombus within the aortic graft in seven patients (19.4%). All were treated with renal artery thrombolysis and placement of relining stents. Additional interventions were performed for a type Ia endoleak (proximal graft extension with placement of visceral chimney grafts in one patient), type II endoleaks (inferior mesenteric artery embolization in two patients), and renal stent compression without occlusion (renal artery angioplasty for three patients). The patients treated with large diameter endografts had a significantly greater incidence of composite thrombotic complications compared with those with small diameter endografts (45.5% vs 7.1%, respectively; $P = .016$). Isolated mural thrombus occurred exclusively in the large diameter cohort vs the small diameter cohort (n = 7 [31.8%] vs n = 0 [0%]; $P = .019$). All thrombotic events had occurred after ≥6 months of follow-up and were not present on the initial postoperative imaging studies from which the 3D models were based.

Effect of endograft diameter on aortic hemodynamics. Quantitative analysis revealed significant differences in aortic TAWSS and RT values between the endograft diameter cohorts (Fig 2**)**. Preoperatively, the mean aortic TAWSS was lower in the large endograft cohort compared with the small endograft cohort (1.72 ± 0.55 dynes/cm^2 vs 3.06 ± 1.02 dynes/cm^2; $P < .001$). Postoperatively, the mean aortic TAWSS remained lower in the patients treated with large

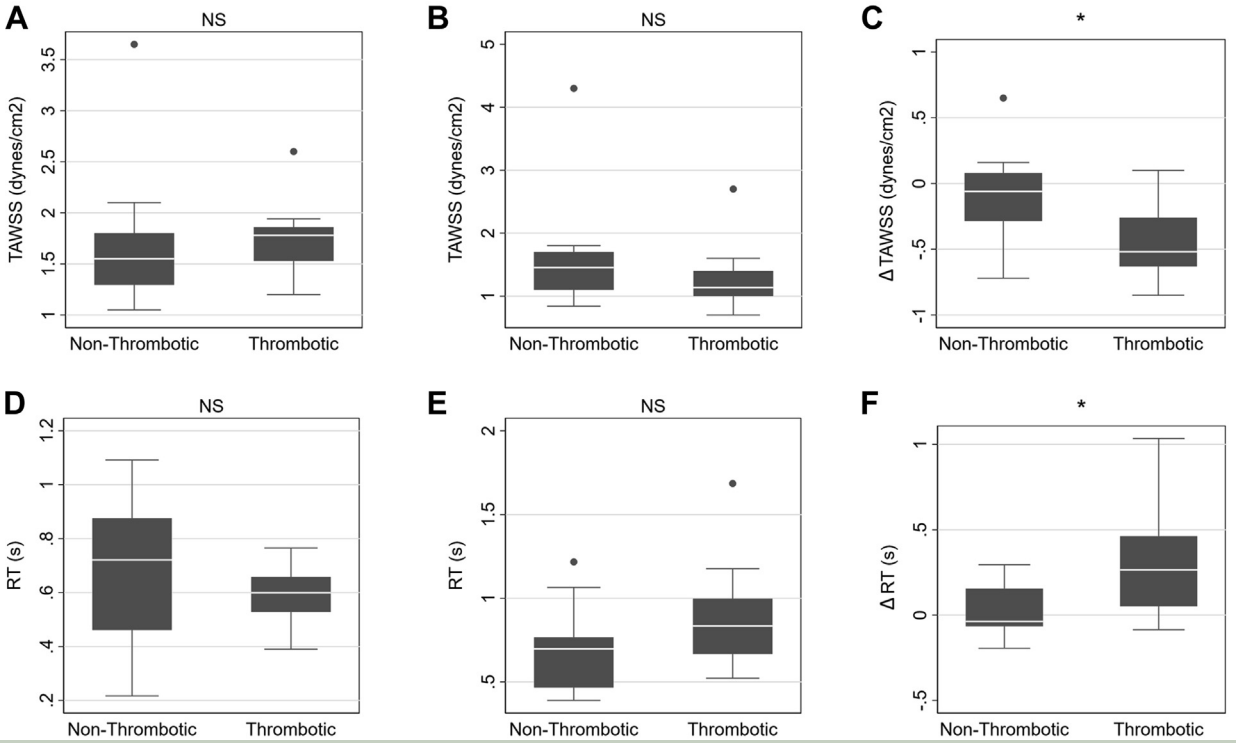

Fig 3. Analysis of aortic hemodynamic metrics for patients treated with large endografts with and without thrombotic complications. **A,** Preoperative aortic time-averaged wall shear stress (TAWSS). **B,** Postoperative TAWSS. **C,** Change in TAWSS (ΔTAWSS). **D,** Preoperative aortic residence time (RT). **E,** Postoperative aortic RT. **F,** Change in aortic RT (ΔRT). *Large,* Large endograft; *NS,* nonsignificant; *Small,* small endograft. *$P < .05$.

endografts (1.45 ± 0.76 dynes/cm^2 vs 3.16 ± 1.24 dynes/cm^2; $P < .001$). Large endografts were more likely to be associated with a postoperative decline in aortic TAWSS, and repair with small endografts was associated with a small increase in the aortic TAWSS (ΔTAWSS, −0.26 ± 0.37 dynes/cm^2 vs 0.10 ± 0.53 dynes/cm^2; $P = .030$). Large endografts were associated with a longer mean RT both preoperatively (0.64 ± 0.21 second vs 0.32 ± 0.08 second; $P < .001$) and postoperatively (0.78 ± 0.30 second vs 0.34 ± 0.08 second; $P < .001$). Treatment with large endografts showed a trend toward a higher RT (ΔRT, 0.14 ± 0.06 second vs 0.01 ± 0.03 second; $P = .09$).

Aortic hemodynamics associated with thrombotic complications in large endografts. Within the large endograft cohort, the aortic hemodynamic values were stratified by the incidence of thrombotic complications (Fig 3). No differences were observed in the mean preoperative aortic TAWSS (1.74 ± 0.39 dynes/cm^2 vs 1.69 ± 0.68 dynes/cm^2; $P = .35$) or postoperative aortic TAWSS (1.28 ± 0.56 dynes/cm^2 vs 1.60 ± 0.91 dynes/cm^2; $P = .25$) between patients with vs without thrombotic complications. Similarly, the mean aortic RT did not significantly differ between patients with vs without thrombotic complications in the preoperative (0.59 ± 0.11 second vs 0.67 ± 0.26 second; $P = .54$) or postoperative (0.89 ± 0.34 second vs 0.69 ± 0.25 second; $P = .11$) models. However, patients with thrombotic complications had had a greater magnitude postoperative reduction in aortic TAWSS (ΔTAWSS, −0.45 ± 0.31 dynes/cm^2 vs −0.09 ± 0.36 dynes/cm^2; $P = .036$) and a larger increase in the aortic RT (ΔRT, 0.29 ± 0.33 second vs 0.02 ± 0.16 second; $P = .023$). Nine patients (90%) with negative TAWSS changes postoperatively had experienced a thrombotic event.

Altered aortic hemodynamics as a predictor of thrombotic complications. Within the large endograft cohort, the aortic ΔTAWSS demonstrated discriminatory power to predict for thrombotic complications (AUC 0.77; 95% confidence interval [CI], 0.56-0.97; Fig 4, *A*). A cutoff value of ≥0.39 dynes/cm^2 decline in TAWSS provided a sensitivity of 70.0% and specificity of 83.3%. A patient-specific aortic ΔRT demonstrated similar accuracy for predicting for thrombotic complications (AUC, 0.78; 95% CI, 0.58-0.98; Fig 4, *B*). A cutoff value of ≥0.05 second increase in RT provided a sensitivity of 80.0% and specificity of 66.7%. The odds of thrombotic complications were significantly higher if fEVAR had reached the threshold ΔTAWSS (OR, 7.0; 95% CI, 1.1-45.9) and ΔRT (OR, 8.0; 95% CI, 1.13-56.8).

3D visualization of areas of low postoperative aortic TAWSS (<0.2 dynes/cm^2) identified the location of maximum thrombus deposition in most patients

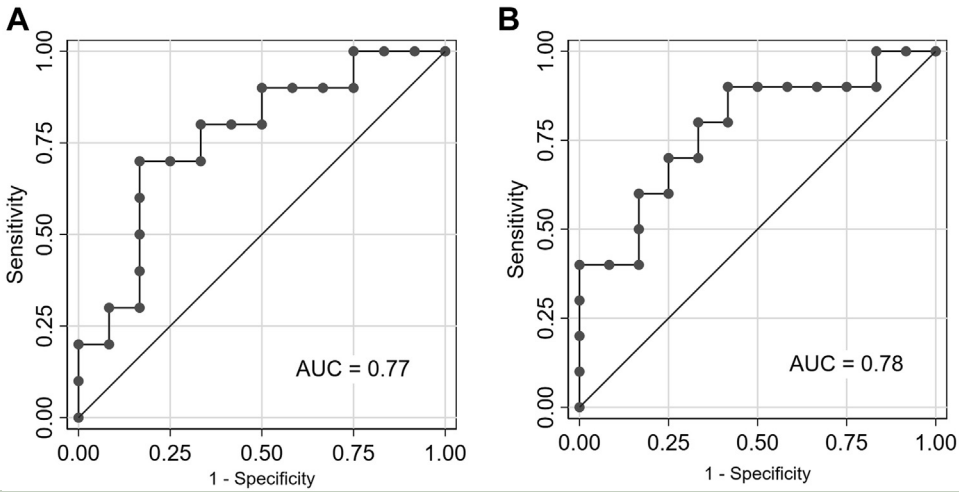

Fig 4. Receiver operating characteristic curve for change in aortic time-averaged wall shear stress (TAWSS; **A**) and change in residence time (RT; **B**) for detection of thrombotic events after fenestrated endovascular aneurysm repair (fEVAR). Both TAWSS and RT cutoff values of ≥0.39 dynes/cm^2 and ≥0.05 second, respectively, demonstrated similar discriminatory power for predicting for thrombotic complications.

(n = 7; 72%) with thrombotic complications. Representative examples of TAWSS visualization in the setting of postoperative aortic thrombus and aortic thrombus with concurrent renal stent occlusion are shown in Figs 5 and 6, respectively.

Effect of endograft diameter on aortic branch hemodynamics. The aortic branch TAWSS values are presented in Supplementary Table I. In the SMA, the postoperative mean TAWSS (16.07 ± 5.87 dynes/cm^2 vs 22.76 ± 6.38 dynes/cm^2; $P = .002$) and ΔTAWSS (−0.91 ± 4.85 dynes/cm^2 vs 1.91 ± 5.23 dynes/cm^2; $P = .042$) was lower in the large vs small endograft cohort. In the renal arteries, repair with large diameter endografts resulted in a negative ΔTAWSS compared with a positive ΔTAWSS after repair with small diameter endografts. This was observed in both the proximal stented (−8.03 ± 8.70 dynes/cm^2 vs +2.88 ± 8.70 dynes/cm^2; $P = .008$) and the distal unstented segments (−3.58 ± 9.75 dynes/cm^2 vs +2.85 ± 10.11 dynes/cm^2; $P = .001$). The renal artery TAWSS values were also stratified and compared by the absence or presence of renal stent occlusion. No significant differences in TAWSS or ΔTAWSS were observed between the two groups (Supplementary Table II).

Computationally derived arterial pressures and flow rates are presented in Supplementary Tables III and IV, respectively. No significant differences were found in the mean or peak arterial pressure in the aorta, celiac artery, SMA, or renal arteries between endograft groups ($P = .06$-$.97$). A higher peak flow was observed in the SMA in both preoperative (50.4 ± 7.7 mL/s vs 42.3 ± 8.3 mL/s; $P = .005$) and postoperative (49.5 ± 7.3 mL/s vs 39.8 ± 7.8 mL/s; $P < .001$) models in the large diameter group. However, no other significant differences were found when comparing the peak or mean flow rates in the aorta, celiac artery, or renal arteries between endograft groups ($P = .24$-$.96$).

DISCUSSION

In the present retrospective patient-specific CFD study, we described key differences in aortic hemodynamics between patients treated with large (34-36 mm) vs small (24-26 mm) diameter Zenith fEVAR endografts. We found that aortic TAWSS was consistently lower and aortic RT consistently higher in patients treated with large vs small endograft diameters. The use of large aortic endografts in fEVAR was also more likely to result in a reduction in aortic TAWSS and increased variability in RT postoperatively. Given the significantly higher incidence of thrombotic complications in the large endograft group, we also explored differences in aortic hemodynamics in patients who had experienced thrombotic complications during the follow-up period. Within the large endograft group, we found that patients with thrombotic issues had had a greater reduction in aortic TAWSS and increase in aortic RT compared with those without thrombotic complications. Patients treated with large endografts meeting the threshold changes in the aorta had had a seven-to eightfold increased risk of future thrombotic events.

Our study findings are particularly relevant given the rapidly evolving landscape of complex endovascular aneurysm repair (EVAR). At present, the Cook Zenith fenestrated endograft is the only U.S. Food and Drug Administration—approved endograft for the treatment of juxtarenal aortic aneurysms. Fenestrated technologies are continuing to expand, with three- and four-vessel fenestrated endografts already available for use in Europe and poised for similar adoption in the United States. Nonetheless, recent studies have reported

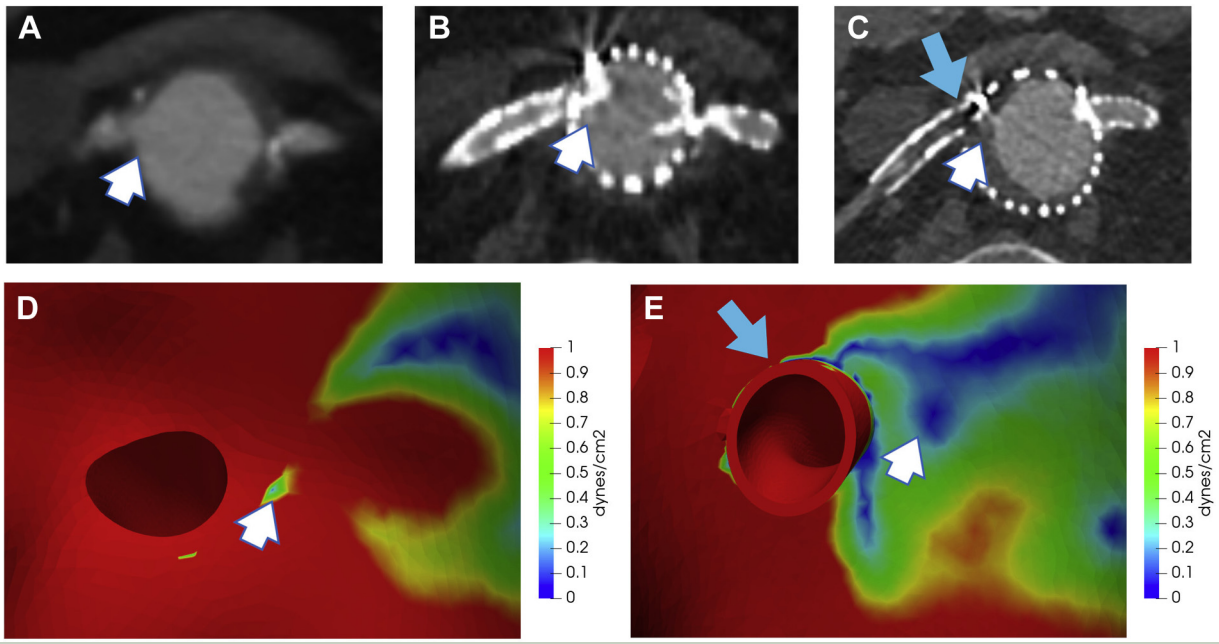

Fig 5. Region of postoperative aortic luminal thrombus (*white arrow*) demonstrated on axial computed tomography on preoperative (**A**), immediate postoperative (**B**), and most recent follow-up (**C**) scans, with corresponding three-dimensional (3D) rendering of time-averaged wall shear stress (TAWSS) in the aortic lumen in preoperatively (**D**) and immediate postoperatively (**E**). The location of thrombus buildup within the posterior aspect of the aortic graft corresponded with areas of very low TAWSS (<0.2 dynes/cm^2) in the postoperative model, which was not present compared with preoperative model.

durability issues, with a 20% risk of late branch-related intervention.[4,22] Our group has previously described the differential reintervention risk associated with large 34- to 36-mm diameter fEVAR endografts.[6] In the present study, we found a nearly threefold incidence of renal stent occlusion in patients treated with large-vs small-diameter endografts. These stent occlusions occurred without evidence of stent compression on CTA, leading us to hypothesize that adverse local hemodynamics might play a role in the increased risk of stent thrombosis. The only patient in the small endograft group to experience a thrombotic complication had developed a renal stent occlusion. On postoperative simulation, this renal stent showed no adverse branch hemodynamic changes. However, it did have areas of very low TAWSS in the region adjacent to the renal flare. We also found that large-diameter fEVAR was associated with a 30% risk of significant luminal graft thrombus developing. In contrast, this finding did not occur in any patients treated with smaller diameter endografts. Although luminal thrombus is both a common and a benign finding for patients treated with standard infrarenal EVAR,[12] the presence of luminal thrombus might be more harmful in the setting of fEVAR owing to the use of flared renal branch grafts. Accordingly, we have presented an example of luminal thrombus that appeared to "stack" around a flared renal stent and, subsequently, might have led to renal stent thrombosis in the absence of renal stent compression. Targeted CFD-based studies evaluating branch occlusion are required to further investigate this phenomenon.

Physiologic wall shear stress in the nondiseased paravisceral abdominal aorta is normally in the range of 2.3 to 5.5 dynes/cm^2 in resting physiologic conditions.[23,24] We found that small diameter fEVAR maintained normal physiologic aortic TAWSS values in this region (~3 dynes/cm^2). However, large diameter fEVAR resulted in a near 50% lower TAWSS (~1.5 dynes/cm^2), reducing the amount of shear forces to below normal physiologic levels. Because the inflow conditions were similar between the two groups (eg, similar blood pressure, heart rate, and allometric scaling), it can be expected that an increasing endograft diameter would correspond to a lower TAWSS. However, we also found that large endografts were significantly more likely to result in a decline in TAWSS postoperatively compared with preoperatively. After reviewing the aortic geometry, no prominent defining features (eg, aortic angulation, tapered or reverse funnel morphology) were found to distinguish fEVAR with a TAWSS decline vs without such a decline. However, the unique benefit of CFD modeling is the ability to capture interactions between a multitude of geometric elements (eg, subtle changes in aortic contour, renal flare geometry) and quantify the resultant downstream hemodynamic effects. Thus, CFD-derived metrics can directly account for all features of aortic anatomy

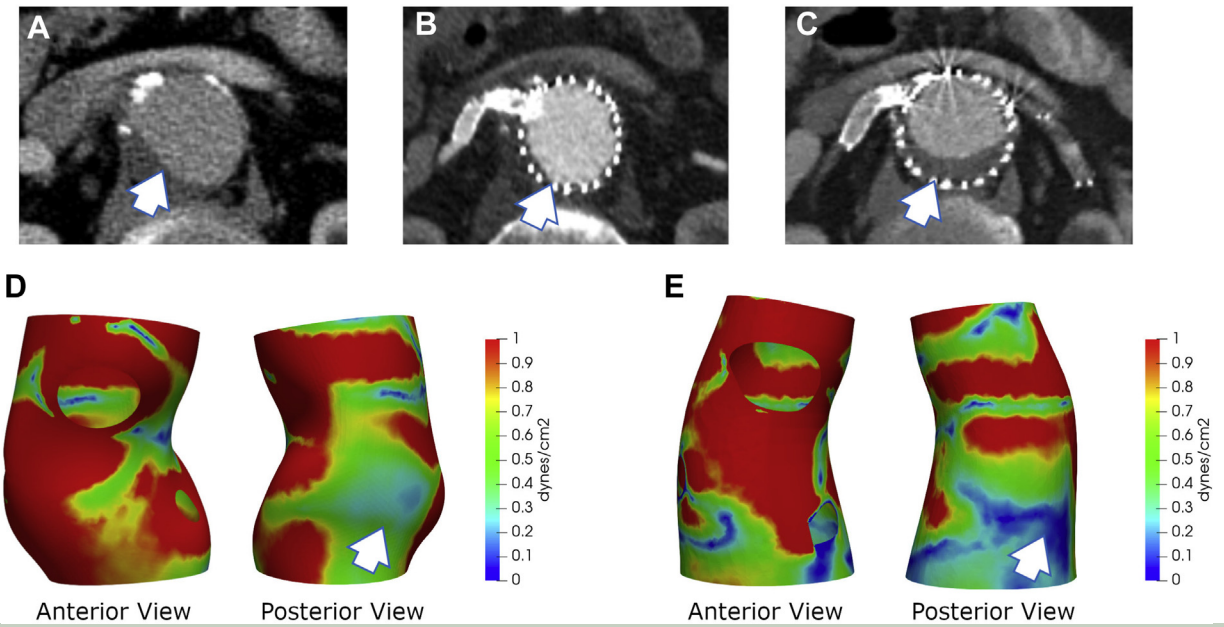

Fig 6. Region of postoperative aortic thrombus (*white arrow*) with associated thrombotic occlusion of right renal stent (*blue arrow*) demonstrated on axial computed tomography imaging on preoperative (**A**), immediate postoperative (**B**), and most recent follow-up (**C**) scans, with corresponding three-dimensional (3D) rendering of time-averaged wall shear stress (TAWSS) in the aortic lumen and right renal orifice preoperatively (**D**) and postoperatively (**E**). The location of thrombus build-up within the right lateral aspect of the aortic graft corresponded to areas of very low TAWSS (<0.2 dynes/cm^2) in the postoperative model, which was not present compared with the preoperative model. In this patient, no structural kinking or stenosis was present within the renal artery, and the TAWSS, pressure, and flow rates in the renal artery were normal.

and are, thus, uniquely advantageous for studying complex aortic endograft geometries. It is possible that the areas of flow stagnation due to flared branch grafts will be more pronounced after treatment with large endografts. Large diameter grafts have also been associated with a higher degree of postoperative neck dilation. Both of these factors could explain why lower TAWSS was observed postoperatively in the paravisceral seal zone after fEVAR with large diameter endografts.[25] Future controlled experiments with idealized geometries and varied endograft diameters and flare geometry might aid in understanding how changes in aortic morphology and stent geometry affect aortic hemodynamics. This could also be an avenue for incorporating animal models to explore various disease conditions and stent graft geometries, which would have the benefit of allowing for model validation using invasive measurement techniques.[26]

Low levels of wall shear stress, associated with low local blood velocity, are well known to be a causal factor in thrombus deposition owing to increasing local blood viscosity, erythrocyte aggregation, and platelet activation.[27–29] Wall shear stress-related indexes have been shown to accurately identify regions of thrombus formation in untreated abdominal aortic aneurysms.[29,30] A recent CFD-based study by Boyd et al[31] found that TAWSS values of <0.2 dynes/cm^2 correlated with future locations of thrombus deposition and eventual aneurysm rupture. In our study, a similar threshold of aortic TAWSS of <0.2 dynes/cm^2 in postoperative simulations identified the location of maximal thrombus deposition in nearly three quarters of cases. This region was often immediately adjacent to a flared renal branch stent and is consistent with areas of altered velocity streamlines and flow recirculation previously attributed to flared renal stent geometry.[14] Kandail et al[10] also studied the effects of flared stent geometry in fEVAR. In controlled computational "bench testing," they found that longer flare lengths and larger flare angles were associated with higher calculated endothelial cell activation potential (ie, areas of low TAWSS), which would serve as a hemodynamic nidus for thrombus formation.[10] We did not find significant differences in aortic and branch outlet pressures between the pre- and postoperative states or endograft diameter groups. Hemodynamic variables that relate to wall stress indexes appear to be more useful for predicting the thrombotic potential compared with other perfusion metrics such as blood pressure or flow rates.[10,32] However, we could not find a correlation between the branch TAWSS and branch occlusion, perhaps owing to the low number of observed renal occlusion events in our cohort.

Flow recirculation zones have also been shown to correlate to areas of platelet accumulation and activation.[29]

Measurement of RT provided a quantifiable metric to assess regions of stagnant flow.[33] Grande Gutierrez et al[32] found that an increased RT and a decreased TAWSS correlated with areas of coronary artery aneurysms prone to thrombosis through platelet accumulation. Tzirakis et al[34] showed that intraluminal thrombosis was more likely to occur in abdominal aortic aneurysms with a higher relative RT. In the present study, a higher RT was also predictive of future thrombotic complications in the setting of aortic geometry changes after fEVAR.

Our study had several limitations. Phase-contrast magnetic resonance imaging (PC-MRI) was not obtained in our study, which would have provided true patient-specific inflow conditions and a method of model validation. However, PC-MRI studies are resource intensive and not routinely performed in our current clinical workflow nor in most aortic practices. PC-MRI would be particularly useful for patients with iliac occlusive disease with significant epigastric and mesenteric and/or pelvic collateral vessels. Inclusion of a subset of patients with PC-MRI–based flow validation would instill more confidence in our hemodynamic findings and is the subject of future investigation. The potential was also present for outcome bias, because the clinical outcome of interest was determined by CTA imaging, which was the same modality used for construction of the 3D flow simulation models. However, only the first postoperative CTA study was used for model derivation, and in our series, these were uniformly free of thrombotic complications, thus reducing the potential for bias from linking postoperative CTA-derived hemodynamics to subsequent CTA-derived clinical outcomes. Another image-related limitation was the inability to capture small graft fabric irregularities, which cannot be visualized using CTA. These could potentially serve as a nidus for thrombus formation but were not adequately represented in our flow simulations. Finally, our simulations assume rigid, nondeformable walls. Although endografts behave as nearly rigid in vivo, native vessels are best modeled using deformable wall simulations using coupled momentum methods to determine fluid–solid interactions. However, this often requires an order of magnitude increase in computational resources.[20] Other studies have also shown minimal differences between rigid and deformable wall simulations on calculated hemodynamic parameters in the abdominal aorta.[35]

Regarding cohort limitations, the low event rate of renal stent occlusions limited the ability to differentiate between unique hemodynamic predictors of renal stent occlusions vs aortic graft thrombus. The present study did not include patients treated with intermediate diameter (28-32 mm) fEVAR endografts. Within our registry, this intermediate cohort consisted of >100 patients. Applying similar selection criteria would have resulted in a cohort size beyond our current available computational resources. We, thus, specifically excluded this group to reduce the potential for selection bias from only selecting a small subset of this intermediate group. Analyzing this intermediate cohort of patients would provide information to determine whether a threshold diameter exists at which adverse aortic hemodynamics occur more frequently. At present, we do not have CFD-derived aortic hemodynamic data for this intermediate population, which is a potential topic of future study.

Multifenestrated and branched EVAR currently represent the forefront of minimally invasive repair of suprarenal and thoracoabdominal aortic aneurysms. Notwithstanding, our understanding of the potential implications of abnormal hemodynamics associated with complex endograft geometries is limited. In the present retrospective study, we have described evidence linking patient-specific CFD-derived aortic hemodynamic values to thrombotic complications in a larger series of patients who had undergone fEVAR. Accurate hemodynamic classification of thrombotic risk could identify patients who might benefit from more frequent surveillance imaging or a longer period of dual antiplatelet or anticoagulation therapy. CFD-based investigations of complex EVAR will become increasingly relevant in the future era of personalized, precision surgery when considering complex aortic aneurysm repair. We believe that these translational studies will provide key hemodynamic insights to form the basis of patient-specific optimized preoperative planning and postoperative risk stratification and potentially guide future advancements in aortic endograft design.

CONCLUSIONS

Patient-specific CFD simulation of fEVAR for juxtarenal abdominal aortic aneurysms demonstrated significant endograft diameter-dependent differences in local aortic hemodynamics. A postoperative reduction in aortic TAWSS and increased aortic RT correlated with the development of intraluminal graft thrombus or renal stent occlusion in patients treated with large diameter endografts and, thus, might be a novel hemodynamic predictor for identifying patients at increased risk of thrombotic complications. Prospective studies are required to further assess the clinical translation of simulated aortic hemodynamics on thrombotic risk stratification after implantation of complex aortic endografts.

AUTHOR CONTRIBUTIONS

Conception and design: KT, AM, RD, JL
Analysis and interpretation: KT, KF, WY, ES
Data collection: KT, KF
Writing the article: KT, KF
Critical revision of the article: KT, KF, WY, ES, AM, RD, JL
Final approval of the article: KT, KF, WY, ES, AM, RD, JL
Statistical analysis: KT

Obtained funding: KT, AM, JL
Overall responsibility: JL

REFERENCES

1. Suckow BD, Goodney PP, Columbo JA, Kang R, Stone DH, Sedrakyan A, et al. National trends in open surgical, endovascular, and branched-fenestrated endovascular aortic aneurysm repair in Medicare patients. J Vasc Surg 2018;67:1690-7.e1.
2. Canavati R, Millen A, Brennan J, Fisher RK, McWilliams RG, Naik JB, et al. Comparison of fenestrated endovascular and open repair of abdominal aortic aneurysms not suitable for standard endovascular repair. J Vasc Surg 2013;57:362-7.
3. de Souza LR, Oderich GS, Farber MA, Haulon S, Banga PV, Pereira AH, et al. Editor's choice — comparison of renal outcomes in patients treated by Zenith® fenestrated and Zenith® abdominal aortic aneurysm stent grafts in US prospective pivotal trials. Eur J Vasc Endovasc Surg 2017;53:648-55.
4. Dossabhoy SS, Simons JP, Diamond KR, Flahive JM, Aiello FA, Arous EJ, et al. Reinterventions after fenestrated or branched endovascular aortic aneurysm repair. J Vasc Surg 2018;68:669-81.
5. Walker J, Kaushik S, Hoffman M, Gasper W, Hiramoto J, Reilly L, et al. Long-term durability of multibranched endovascular repair of thoracoabdominal and pararenal aortic aneurysms. J Vasc Surg 2019;69:341-7.
6. Deslarzes-Dubuis C, Stern JR, Tran K, Colvard BD, Anahita D, Lee JT. Fenestrated endovascular repair with large device diameters (34- to 36-mm) is associated with increased rates of type 1 and 3 endoleak and reintervention. Eur J Vasc Endovasc Surg 2019;58:e861-2.
7. Zarins CK, Taylor CA, Min JK. Computed fractional flow reserve (FFT_{CT}) derived from coronary CT angiography. J Cardiovasc Transl Res 2013;6:708-14.
8. Malinauskas RA, Hariharan P, Day SW, Herbertson LH, Buesen M, Steinseifer U, et al. FDA benchmark medical device flow models for CFD validation. ASAIO J 2017;63:150-60.
9. Steinman DA, Migliavacca F. Editorial: special issue on verification, validation, and uncertainty quantification of cardiovascular models: towards effective VVUQ for translating cardiovascular modelling to clinical utility. Cardiovasc Eng Technol 2018;9:539-43.
10. Kandail H, Hamady M, Xu XY. Effect of a flared renal stent on the performance of fenestrated stent-grafts at rest and exercise conditions. J Endovasc Ther 2016;23:809-20.
11. Kandail H, Hamady M, Xu XY. Comparison of blood flow in branched and fenestrated stent-grafts for endovascular repair of abdominal aortic aneurysms. J Endovasc Ther 2015;22:578-90.
12. Oliveira NFG, Bastos Gonçalves FM, Hoeks SE, Ten Raa S, Ultee KHJ, Rouwet E, et al. Clinical outcome and morphologic determinants of mural thrombus in abdominal aortic endografts. J Vasc Surg 2015;61:1391-8.
13. Les AS, Yeung JJ, Schultz GM, Herfkens RJ, Dalman RL, Taylor CA. Supraceliac and infrarenal aortic flow in patients with abdominal aortic aneurysms: mean flows, waveforms, and allometric scaling relationships. Cardiovasc Eng Technol 2010;1:10.
14. Tran K, Yang W, Marsden A, Lee JT. Patient-specific computational flow modelling for assessing hemodynamic changes following fenestrated endovascular aneurysm repair. J Vasc Surg 2020;72:e182-3.
15. Updegrove A, Wilson NM, Merkow J, Lan H, Marsden AL, Shadden SC. SimVascular: an open source pipeline for cardiovascular simulation. Ann Biomed Eng 2017;45:525-41.
16. Tran K, Feliciano K, Yang W, Marsden A, Dalman R, Lee J. Patient-specific changes in aortic hemodynamics are associated with thrombotic risk after fenestrated endovascular aneurysm repair with large diameter endografts. [e-pub ahead of print]. JVS Vasc Sci, https://doi.org/10.1016/J.JVSSCI.2021.09.021. Accessed December 20, 2021.
17. Vignon-Clementel IE, Figueroa CA, Jansen KE, Taylor CA. Outflow boundary conditions for 3D simulations of non-periodic blood flow and pressure fields in deformable arteries. Comput Methods Biomech Biomed Engin 2010;13:625-40.
18. Segalova PA, Venkateswara Rao KT, Zarins CK, Taylor CA. Computational modeling of shear-based hemolysis caused by renal obstruction. J Biomech Eng 2012;134:1-7.
19. Williams LR, Leggett RW. Reference values for resting blood flow to organs of man. Clin Phys Physiol Meas 1989;10:187-217.
20. Figueroa CA, Vignon-Clementel IE, Jansen KE, Hughes TJR, Taylor CA. A coupled momentum method for modeling blood flow in three-dimensional deformable arteries. Comput Methods Appl Mech Eng 2006;195:5685-706.
21. Esmaily-Moghadam M, Hsia TY, Marsden AL. A non-discrete method for computation of residence time in fluid mechanics simulations. Phys Fluids 2013;25:1-21.
22. Marzelle J, Presles E, Becquemin JP. Results and factors affecting early outcome of fenestrated and/or branched stent grafts for aortic aneurysms: a multicenter prospective study. Ann Surg 2015;261:197-206.
23. Cheng CP, Parker D, Taylor CA. Quantification of wall shear stress in large blood vessels using Lagrangian interpolation functions with cine phase-contrast magnetic resonance imaging. Ann Biomed Eng 2002;30:1020-32.
24. Les AS, Shadden SC, Figueroa CA, Park JM, Tedesco MM, Herfkens RJ, et al. Quantification of hemodynamics in abdominal aortic aneurysms during rest and exercise using magnetic resonance imaging and computational fluid dynamics. Ann Biomed Eng 2010;38:1288-313.
25. Kret MR, Tran K, Lee JT. Change in aortic neck diameter after endovascular aortic aneurysm repair. Ann Vasc Surg 2017;43:115-20.
26. Acuna A, Berman AG, Damen FW, Meyers BA, Adelsperger AR, Bayer KC, et al. Computational fluid dynamics of vascular disease in animal models. J Biomech Eng 2018;140. 0808011-14.
27. Snabre P, Bitbol M, Mills P. Cell disaggregation behavior in shear flow. Biophys J 1987;51:795-807.
28. Nesbitt WS, Westein E, Tovar-Lopez FJ, Tolouei E, Mitchell A, Fu J, et al. A shear gradient-dependent platelet aggregation mechanism drives thrombus formation. Nat Med 2009;15:665-73.
29. Bluestein D, Niu L, Schoephoerster RT, Dewanjee MK. Steady flow in an aneurysm model: correlation between fluid dynamics and blood platelet deposition. J Biomech Eng 1996;118:280-6.
30. Zambrano BA, Gharahi H, Lim C, Jaberi FA, Choi J, Lee W, et al. Association of intraluminal thrombus, hemodynamic forces, and abdominal aortic aneurysm expansion using longitudinal CT images. Ann Biomed Eng 2016;44:1502-14.
31. Boyd AJ, Kuhn DCS, Lozowy RJ, Kulbisky GP. Low wall shear stress predominates at sites of abdominal aortic aneurysm rupture. J Vasc Surg 2016;63:1613-9.
32. Grande Gutierrez N, Mathew M, McCrindle BW, Trans JS, Kahn AM, Burns JC, et al. Hemodynamic variables in aneurysms are associated with thrombotic risk in children with Kawasaki disease. Int J Cardiol 2019;281:15-21.
33. Suh GY, Les AS, Tenforde AS, Shadden SC, Spilker RL, Yeung JJ, et al. Quantification of particle residence time in abdominal aortic aneurysms using magnetic resonance imaging and computational fluid dynamics. Ann Biomed Eng 2011;39:864-83.
34. Tzirakis K, Kamarianakis Y, Metaxa E, Kontopodis N, Ioannou CV, Papaharilaou Y. A robust approach for exploring hemodynamics and thrombus growth associations in abdominal aortic aneurysms. Med Biol Eng Comput 2017;55:1493-506.
35. Looyenga EM, Gent SP. Examination of fluid-structure interaction in stent grafts and its hemodynamic implications. BIOMED; 2018. :V001T08A007.

Submitted Dec 29, 2021; accepted Apr 6, 2022.

Supplementary Table I. Computationally derived time-averaged wall shear stress (TAWSS) within aortic branches

	Preoperative			Postoperative			Change		
TAWSS, dynes/cm^2	Small endograft	Large endograft	*P* value[a]	Small endograft	Large endograft	*P* value[a]	Small endograft	Large endograft	*P* value[a]
Celiac artery	18.97 ± 5.61	24.76 ± 14.36	.19	20.52 ± 6.10	25.08 ± 15.24	.73	1.54 ± 5.29	0.32 ± 8.44	.34
SMA	20.85 ± 6.23	16.98 ± 5.99	.08	22.76 ± 6.38	16.07 ± 5.87	**.002**	1.91 ± 5.23	-0.91 ± 4.85	**.042**
Renal arteries									
Stented (proximal)	22.98 ± 9.25	26.58 ± 13.45	.18	20.10 ± 6.07	18.54 ± 6.83	.20	2.88 ± 8.70	−8.03 ± 12.37	**.008**
Unstented (distal)	29.03 ± 11.8	33.17 ± 12.62	.09	31.89 ± 13.26	29.59 ± 13.02	.36	2.85 ± 10.11	−3.58 ± 9.75	**.001**

Change, Mean paired difference in pre- and postoperative TAWSS per patient; *SMA*, superior mesenteric artery.
Data presented as mean ± standard deviation.
Boldface *P* values represent statistical significance.
[a] *P* values obtained from the Student *t* test or Wilcoxon rank sum test for normally distributed or skewed data, respectively.

Supplementary Table II. Computationally derived time-averaged wall shear stress (TAWSS) in renal arteries stratified by spontaneous late renal stent occlusion (left and right renal arteries were aggregated for this analysis)

Renal artery TAWSS, dynes/cm^2	Uncomplicated (n = 67)	Renal stent occlusion (n = 5)	*P* value
Stented (proximal)			
Preoperative	24.9 ± 12.2	28.1 ± 10.2	.38
Postoperative	19.1 ± 6.7	19.3 ± 2.3	.50
Change	−5.8 ± 11.4	−8.8 ± 10.1	.38
Unstented (distal)			
Preoperative	31.5 ± 12.8	31.9 ± 4.4	.60
Postoperative	30.0 ± 10.2	36.4 ± 10.5	.16
Change	−1.5 ± 10.2	4.5 ± 12.1	.28

Data presented as mean ± standard deviation.

Supplementary Table III. Computationally derived peak and mean arterial pressures

Variable	Preoperative			Postoperative			Change		
	Small endograft	Large endograft	*P* value[a]	Small endograft	Large endograft	*P* value[a]	Small endograft	Large endograft	*P* value[a]
Peak arterial pressure, mm Hg									
Celiac artery	120.4 ± 10.2	120.0 ± 16.6	.94	120.2 ± 8.9	119.2 ± 21.2	.86	−0.2 ± 5.4	−0.8 ± 11.2	.84
SMA	120.4 ± 11.2	128.6 ± 15.1	.09	118.3 ± 11.3	127.7 ± 15.2	.06	−2.1 ± 6.1	−0.9 ± 7.8	.63
Renal arteries	121.8 ± 10.3	125.0 ± 17.7	.39	123.2 ± 12.7	126.7 ± 15.5	.32	1.3 ± 4.8	1.7 ± 6.9	.82
Distal aorta	131.7 ± 8.5	136.7 ± 16.2	.29	133.8 ± 11.1	136.4 ± 17.2	.61	2.1 ± 4.2	−0.3 ± 3.4	.07
Mean arterial pressure, mm Hg									
Celiac artery	93.8 ± 6.2	93.8 ± 11.4	.97	93.7 ± 6.2	92.8 ± 13.5	.81	−0.1 ± 1.8	−0.9 ± 4.8	.55
SMA	93.5 ± 6.2	95.9 ± 11.1	.47	92.8 ± 6.4	95.6 ± 11.3	.41	−0.7 ± 2.0	−0.3 ± 2.3	.61
Renal arteries	93.7 ± 6.5	94.6 ± 12.2	.72	93.8 ± 6.8	95.4 ± 11.2	.53	0.2 ± 1.2	0.8 ± 3.2	.37
Distal aorta	96.8 ± 5.7	98.4 ± 11.3	.62	97.3 ± 5.7	98.3 ± 11.7	.75	0.5 ± 0.8	0.1 ± 1.1	.12

Change, Mean paired difference in pre- and postoperative pressures per patient; *SMA*, superior mesenteric artery.
Data presented as mean ± standard deviation.
[a] *P* value obtained using the Student *t* test.

Supplementary Table IV. Computationally derived peak and mean arterial flow rates

Variable	Preoperative			Postoperative			Change		
	Small endograft	Large endograft	*P* value[a]	Small endograft	Large endograft	*P* value[a]	Small endograft	Large endograft	*P* value[a]
Peak flow rate, mL/s									
Celiac artery	37.4 ± 7.4	37.3 ± 9.5	.96	37.4 ± 8.9	37.8 ± 12.1	.94	0.08 ± 4.57	0.49± 8.91	.87
SMA	42.3 ± 8.3	50.4 ± 7.7	**.005**	39.8 ± 7.8	49.5 ± 7.3	**<.001**	2.58 ± 5.46	−0.88 ± 7.88	.48
Renal arteries	15.0 ± 2.9	15.8 ± 3.2	.27	15.3 ± 3.2	16.2 ± 3.0	.24	0.28 ± 1.03	0.34 ± 1.36	.86
Distal aorta	85.2 ± 18.0	84.4 ± 16.9	.90	87.5 ± 18.9	84.4 ± 19.1	.64	2.33 ± 5.83	0.01 ± 4.55	.18
Mean flow rate, mL/s									
Celiac artery	8.0 ± 1.3	8.3 ± 1.2	.59	8.0 ± 1.3	8.2 ± 1.3	.73	0.01 ± 0.14	−0.08 ± 0.39	.53
SMA	9.8 ± 1.5	10.1 ± 1.4	.39	9.7 ± 1.5	10.2 ± 1.3	.32	0.09 ± 0.19	−0.04 ± 0.25	.44
Renal arteries	7.1 ± 1.0	7.3 ± 1.0	.50	7.2 ± 1.0	7.4 ± 1.0	.38	0.01 ± 0.08	0.06 ± 0.26	.36
Distal aorta	15.9 ± 3.8	16.8 ± 3.5	.50	16.1 ± 3.8	16.8 ± 3.5	.55	0.08 ± 0.14	−0.01 ± 0.21	.20

Change, Mean paired difference in pre- and postoperative pressures per patient; *SMA*, superior mesenteric artery.
Data presented mean ± standard deviation.
Boldface *P* values represent statistical significance.
[a] *P* value obtained using the Student *t* test.